Optics Letters

Silicon microring modulator-based RF mixer for millimeter-wave phase-coded signal generation

YIWEI XIE,[1] LEIMENG ZHUANG,[1,*] AND ARTHUR JAMES LOWERY[1,2]

[1]Electro-Photonics Laboratory, Department of Electrical and Computer Systems Engineering, Monash University, Clayton, VIC 3800, Australia
[2]Centre for Ultrahigh-bandwidth Devices for Optical Systems (CUDOS), Monash University, Clayton, VIC 3800, Australia
*Corresponding author: leimeng.zhuang@monash.edu

Received 8 May 2017; revised 15 June 2017; accepted 19 June 2017; posted 20 June 2017 (Doc. ID 295117); published 7 July 2017

Phase-coded radio frequency (RF) pulses are widely adopted for radar systems as an effective signal format to enable high-range resolution. However, generating such signals conventionally requires high-speed electronics and complex RF circuitry that impose burdens on the system cost and power consumption. In particular, modern radar systems desire features such as high frequencies, e.g., in the millimeter-wave region, high compactness, and high system flexibility, which pose great challenges for the conventional all-electronics solutions. In contrast, integrated microwave photonics opens a way to solutions that are able to provide those features simultaneously, together with potential for full integration and low cost fabrication. Here, we present an integrated microwave photonic method of a binary-phase-coded millimeter-wave signal generation. The core device is a silicon microring modulator with a device size of 0.13 mm × 0.32 mm and a modulation bandwidth of 23 GHz. Using RF seed frequencies of 17.5 GHz and 20 GHz, respectively, we experimentally demonstrated the generation of binary-phase-coded signals at 35 GHz and 40 GHz using our proposed approach, the performance of which was verified by a pulse compression ratio of 94 and 106, respectively. The result of this work points to the realization of a chip-scale flexible millimeter-wave signal generator.

OCIS codes: (130.0130) Integrated optics; (320.5520) Pulse compression; (350.4010) Microwaves; (060.5625) Radio frequency photonics.

https://doi.org/10.1364/OL.42.002742

In modern radar systems, pulse compression techniques have been widely employed to improve the range resolution [1]. A well-known technique is to use phase-coded RF pulses. Conventionally, such signals can be synthesized by phase-modulating an RF tone, using an analog mixer or a quadrature modulator [2]. For high-frequency cases, e.g., in the millimeter-wave region, frequency multipliers may be used to obtain the RF tones. While analog electronics feature industry maturity and have been deployed in many applications, synthesizing such signals using optical approaches is of high interest for applications such as antenna remoting [3]. This is because the signal synthesis and delivery can be both implemented in the optical domain, which benefits the system with respect to antenna coverage and complexity.

To date a number of optical approaches for generating phase-coded RF pulses have been demonstrated [4–11], including the use of an optical phase modulator in a Sagnac loop [4], Mach–Zehnder interferometer-based modulators [5–7], polarization modulators [8], and Bragg grating-based waveform synthesizers [9,10]. All these works demonstrated RF frequencies in the order of tens of GHz and frequency tunability. In recent years, silicon microring modulators (MRMs) have been developed for optical communication applications, and their modulation bandwidth and efficiency are rapidly improving [11]. Such a device is also able to be applied for the generation of RF phase-coded signals.

Here, we propose and experimentally demonstrate an optical approach for RF phase-coded signal generation. The core device is a silicon MRM, with a device size of 0.13 mm × 0.32 mm and a modulation bandwidth of 23 GHz, which operates in association with a Mach–Zehnder modulator (MZM) and a photodiode (PD). In effect, it performs as an equivalent to a serial cascade of a RF frequency doubler and a mixer that maps a digital control signal to binary phase coding. In a proof-of-concept experiment, we demonstrated the generation of binary-phase-coded RF signals at 35 GHz and 40 GHz, respectively, with corresponding phase coding rates of 8.75 Gbit/s and 10 Gbit/s. To show the effect of phase coding for the purpose of pulse compression, we calculated the autocorrelation compression ratios of the generated RF signals at a length of 128 coding bits pseudo-random bit sequence (PRBS) pattern. The results show a compression ratio of 94 for the 35 GHz signal and 106 for the 40 GHz signal.

Figure 1 shows the system working principle. Different from the traditional electrical methods of generating the phase-coded signal, as shown in Fig. 1(a), our approach uses a serial cascade of an MZM, an MRM, and a PD. In Fig. 1(b), the MZM is fed with a CW light and is biased at the minimum transmission point in order to implement a double-sideband suppressed-carrier spectrum. When driven by an RF seed frequency, f_{in}, and assuming that only the first-order modulation sidebands have significant powers under a small-signal condition, the optical

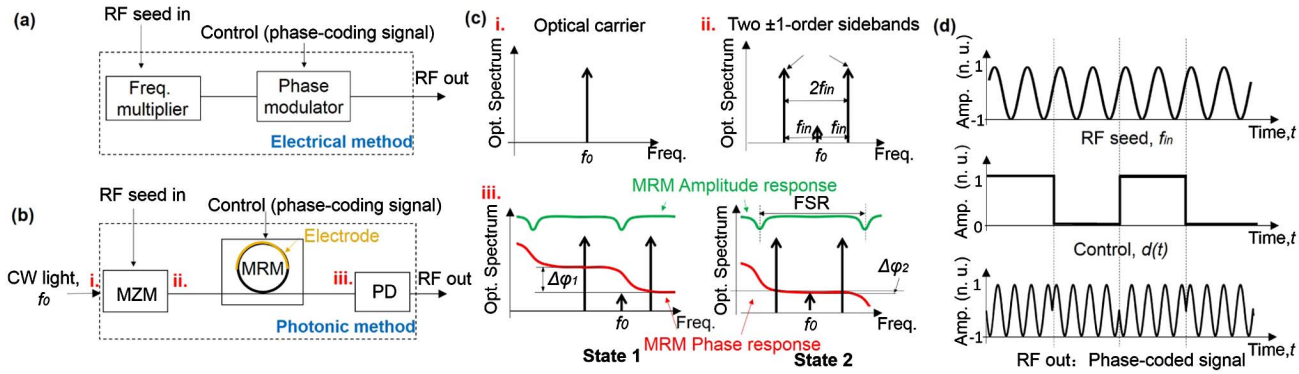

Fig. 1. Schematic of the phase-coded pulse generation system using (a) electrical method and (b) proposed photonic method. (c) Frequency-domain illustration of the system working principle. (d) Time-domain illustration of the signal waveforms.

spectrum at the MZM output will comprise two optical tones with a frequency spacing of $2f_{\text{in}}$, as illustrated in Fig. 1(c). This modulator output field, $E_{\text{MZM}}(t)$, can be expressed by

$$E_{\text{MZM}}(t) = A_{-1}\exp[j2\pi(f_0 - f_{\text{in}})t] + A_{+1}\exp[j2\pi(f_0 + f_{\text{in}})t], \quad (1)$$

where f_0 is the frequency of the CW light, and $A_{\pm 1}$ are the amplitude coefficients determined by the input optical power and modulation depth. This signal is then sent as the input to the MRM, which has a frequency response $H_{\text{MRM}}(f)$:

$$H_{\text{MRM}}(f) = \frac{\sqrt{1-\kappa} - \sqrt{\alpha}e^{-j(\theta+m)}}{1 - \sqrt{\alpha(1-\kappa)}e^{-j(\theta+m)}}, \quad (2)$$

where $\theta(f) = 2\pi f/\Delta f_{\text{FSR}}$ is the phase response to an input frequency, f, normalized to the free spectral range (FSR), Δf_{FSR}, of the resonator, α and κ are the resonator roundtrip loss and power coupling ratio, respectively, and $m(t) = \pi d(t)/V_\pi$ is a phase shift determined by a modulating signal, $d(t)$, in volt and modulator half-wave voltage, V_π [12]. We assume that $d(t)$ is a binary digital signal, and its two voltage levels result in two different MRM frequency responses, as illustrated in Fig. 1(c). Then, when the input optical spectrum to the MRM, i.e., the two optical tones are frequency-aligned with the two MRM frequency responses, as illustrated in Fig. 1(c), the MRM-introduced phase shift difference between the two optical tones, $\Delta\varphi$, will switch between two different values, $\Delta\varphi_1$ and $\Delta\varphi_2$, according to the bit-pattern of the digital control signal. The optical signal field at the output of the MRM, $E_{\text{MRM}}(t)$, can be expressed by

$$\begin{aligned} E_{\text{MRM}}(t) = {} & A_{-1}|H_{RR}(f_0 - f_{\text{in}})|\exp[j2\pi(f_0 - f_{\text{in}})t \\ & + \varphi(f_0 + f_{\text{in}}) + \Delta\varphi(d(t))] \\ & + A_1|H_{RR}(f_0 + f_{\text{in}})|\exp[j2\pi(f_0 + f_{\text{in}})t \\ & + \varphi(f_0 + f_{\text{in}})]. \end{aligned} \quad (3)$$

Then, by means of photodetection, the beating between the two optical tones in association with the switching between $\Delta\varphi_1$ and $\Delta\varphi_2$ will result in the generation of a binary-phase-coded RF signal with a frequency of $2f_{\text{in}}$. A time-domain illustration of this is shown in Fig. 1(d). The output RF signal in the photocurrent can be expressed by

$$\begin{aligned} i(t) = {} & RA_1A_{-1}|H_{RR}(f_0 - f_{\text{in}})||H_{RR}(f_0 + f_{\text{in}})| \\ & \times \cos[2\pi(2f_{\text{in}})t + \Delta\varphi(d(t))], \end{aligned} \quad (4)$$

where R is the responsivity of the PD.

With respect to the operation range of f_{in}, three boundary conditions are considered. For one thing, f_{in} and $2f_{\text{in}}$ must, respectively, fall within the bandwidth of the MZM and PD. Second, $2f_{\text{in}}$ should deviate from being a multiple integer of the FSR of the MRM to allow for a value difference between $\Delta\varphi_1$ and $\Delta\varphi_2$. Last, for the optimization of the phase coding effect, $2f_{\text{in}}$ should be wider than the sharp-change region in the MRM's phase response so as to maximize the difference between $\Delta\varphi_1$ and $\Delta\varphi_2$. The total phase shift span and width of this sharp-change region is determined by κ of the MRM [12]. In addition, the two optical sidebands should avoid the notch-shaped loss of the MRM's amplitude response to minimize the amplitude variation in the generated RF signal.

Figure 2(a) shows a photomicrograph of the silicon MRM and PD. The device was fabricated on a silicon-on-insulator wafer with 200 nm top silicon and 2 μm buried oxide at IMEC [13], using a multi-project wafer foundry fabrication shuttle run under the ePIXfab ISIPP25G silicon technology platform. The MRM consists of a ring resonator waveguide architecture with a radius of 7.5 μm, which is coupled to a bus waveguide with a gap of approximately of 200 nm, resulting in a κ about 0.5. The MRM has a FSR of about 160 GHz (12.9 nm) and a waveguide loss of about 35 dB/cm. A symmetric lateral PN diode is embedded along the ring resonator waveguide to enable modulation of the refractive index, thus modifying the MRM frequency response, i.e., shifting its resonant frequency. A thermal tuning section is formed by a separate p-doped resistor near the coupling region for coarse tuning. The PD is implemented using an IMEC standard very-high-speed germanium (Ge) building block; its typical responsivity is 0.45 A/W, and its dark current is lower than 15 nA. Figures 2(b) and 2(c) show the device electro-optical bandwidth measurements. The 3 dB bandwidths of MRM and PD were measured to be 23 GHz and 50 GHz, respectively. Under reverse bias, the MRM operates with a high-speed free-carrier depletion mode, guaranteeing high modulation bandwidth. While, in the forward bias mode, the carrier density in the MRM increases significantly with the bias voltage, which allows for smaller V_π. In this work, we operated the MRM in the forward bias mode to lower the voltage requirement of the control signal.

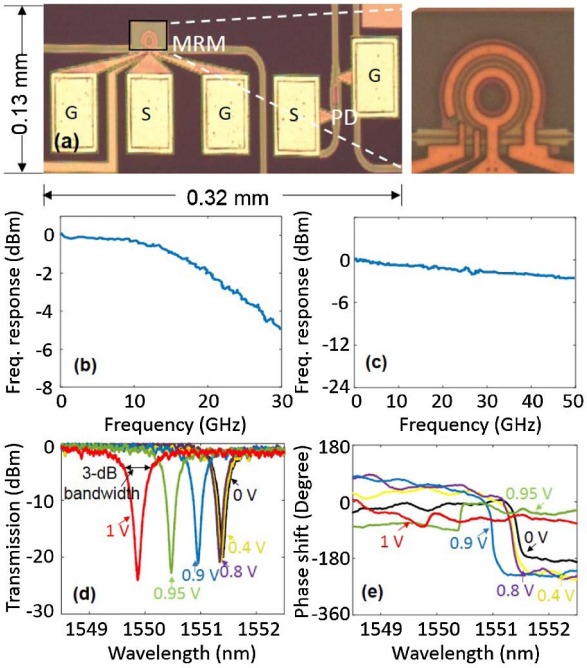

Fig. 2. (a) Photomicrograph of the silicon microring modulator and photodiode. (b), (c) Electro-optical bandwidth measurements of the MR and photodiode (with a bias of −2 V). (d), (e) Measured power transmissions and phase responses of the MR for different bias voltages.

The amplitude and phase responses of the MRM at different bias voltages are shown in Figs. 2(d) and 2(e), respectively, which were measured using a LUNA two-port optical analyzer (VOA5000 with a resolution of 160 MHz). The amplitude notch bandwidth is about 30 GHz (0.24 nm). By tuning the bias voltage from 0 V to 1 V, the MRM resonance frequency shifts by 187 GHz (1.5 nm). The bias voltages of 0.95 V are slightly over the breakdown voltage of the MRM, which causes significant charge carrier flow through the waveguide. In effect, this induces higher roundtrip loss of the ring and thereby renders the MRM in the undercoupling status instead of regular overcoupling status when the bias is between 0 and 0.8 V.

Figure 3 illustrates the experimental setup of the proposed binary-phase-coded signal generation system. An external intensity modulator (LN05S-FC) was used to modulate an RF seed frequency (Rohde & Schwarz SMF 100A) onto a CW light from an external cavity laser (TLG-300). The modulator was biased at minimum transmission to implement double-sideband suppressed-carrier modulation. The measured output spectrum comprising two optical tones is shown by the green lines in Fig. 4. The intensity modulator is able to be biased to yield a double-sideband suppressed-carrier spectrum with sideband-carrier ratio about 30 dB. This modulated optical signal was then coupled into the MRM via a grating coupler optimized for TE polarization, where an erbium-doped fiber amplifier and a polarization controller were used to provide an optical power of 10 dBm at the input of the MRM. The fiber coupler-in and -out loss is about 9 dB, and the MRM loss is about 3 dB. Figure 4(a) shows the MRM frequency responses at the MRM biases of 0 V and 1 V, in relation to the frequency positions of the two optical tones passing the MRM. The frequency responses of MRM under biases of

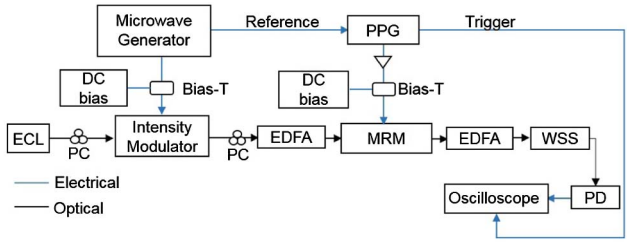

Fig. 3. Experimental setup of the proposed mm wave phase-coding system. (ECL, external cavity laser; PC, polarization controller; PPG, pulse pattern generator).

0 V and 1 V are normalized to the maximum transmission power. Figure 4(b) shows that the MRM's introduced phase shift difference between the two optical tones is about 170° for the MRM bias at 0 V and about 0° for the bias at 1 V.

For the signal generation experiment, an RF seed frequency of 17.5 GHz was first applied to the intensity modulator. When no control signal is applied to the MRM, a continuous sinusoidal RF signal with a frequency of 35 GHz was generated at the system output, measured by a real-time 50 GHz oscilloscope (Agilent DSO-X-95004Q) and is shown in Fig. 5(a). Then, a binary control signal at 8.75 Gb/s with a pattern of "010101" sequence and a peak–peak voltage of 1 V was applied to drive the MRM. Here, the bit rate of the binary signal is chosen to be a quarter of the generated RF frequency. This results in the generation of a phase-modulated waveform, as shown in Fig. 5(b). The resulting phase change in the generated signal can be calculated by means of Hilbert transform, and the result is shown in Fig. 5(c). To demonstrate the frequency flexibility of the system, the same measurements were repeated with an RF seed frequency of 20 GHz and a binary control signal at 10 Gb/s. This results in the generation of a phase-coded signal with a frequency of 40 GHz, whose waveforms with or without the control signal and the phase change are shown in Figs. 5(d), 5(e), and 5(f), respectively.

Figures 5(b) and 5(e) show that the amplitude of the generated signal decreases at the phase changes. This is mainly because when the binary control signal drives the MRM switches between the two frequency responses, the amplitude notch will move from between the two optical tones to out of them or vice versa, which suppresses one of them on its path, resulting in a decrease of amplitude in the generated RF signal. Besides, the dynamics of the MRM when switching between two steady resonance statuses also contributes to the amplitude

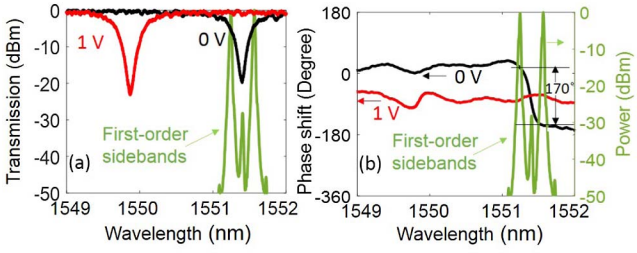

Fig. 4. (a) Power transmissions and (b) phase responses of the MR at bias voltages of 0 V (black) and 1 V (red) and measured spectrum of the modulated optical signal with two first-order sidebands spaced at 40 GHz (green).

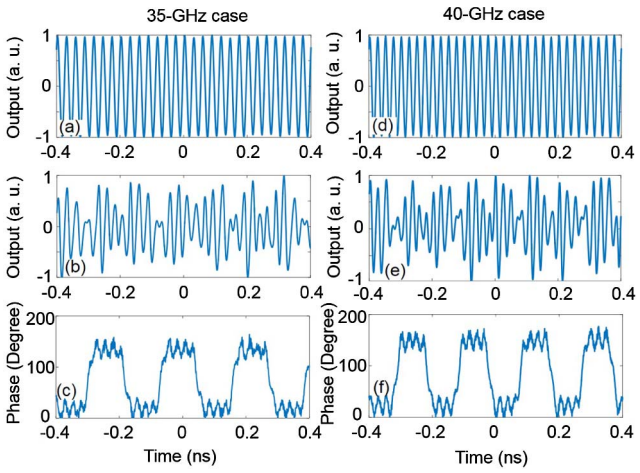

Fig. 5. Waveform measurements of generated RF signals at 35 GHz and 40 GHz modulated by a square wave phase signal: (a), (d) carriers without phase coding; (b), (e) signals with phase coding; and (c), (f) the recovered phase from the phase-coded signals.

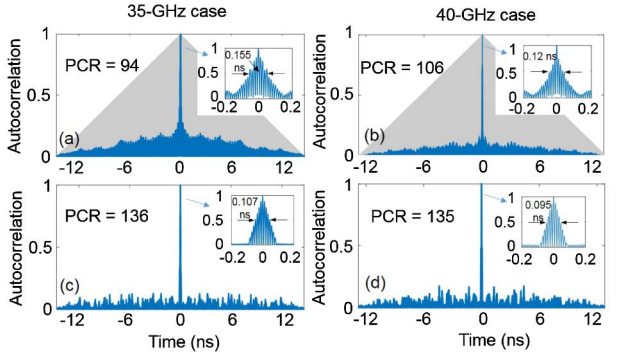

Fig. 6. (a), (b) Calculated autocorrelations of the phase-coded RF pulses using proposed method at 35 GHz and 40 GHz, phase coded by PRBS signals (blue) and the autocorrelations of the uncoded RF pulse at 35 GHz and 40 GHz (grey). (c), (d) Autocorrelations of the phase-coded RF pulses at 35 GHz and 40 GHz in ideal cases. (Insets: zoom in autocorrelations of the phase-coded RF pulse peaks).

variation of the generated RF signal. Figures 5(c) and 5(f) show the effective binary phase coding of the generated RF signals, i.e., 155° for 35 GHz and 170° for 40 GHz, respectively, which are acquired by means of Hilbert transform. The results are in good agreement with the MRM's phase responses shown in Fig. 4(b) and thereby prove the working principle of the proposed system. The ripples of the phase change can be improved by reducing the amplitude difference between switching sections and higher bandwidth of the MRM.

Further, to show the effect of phase coding for the purpose of pulse compression, we generated general-pattern binary-phase-coded RF signals at 35 GHz and 40 GHz, using PRBS signals (SHF BPG 44E) as the MRM driving signal. The PRBS bit rate was chosen to be a quarter of the output RF frequencies. The phase shift difference between "+1" and "−1" determines the capability of pulse compression [4]. Then, we calculated the autocorrelations of generated RF waveforms at a length of 128 bits. Figure 6(a) shows the calculated results in the form of compressed pulses, where the inset shows the zoom-in view of the pulse peak. For the 35 GHz case, a compressed pulse with an FWHM of about 0.155 ns is obtained in comparison with a RF waveform length of 14.6 ns. This means a pulse compression ratio (PCR) of 94. Likewise, Fig. 6(b) shows the 40 GHz case, where a pulse peak FWHM of 0.12 ns is obtained against an RF waveform length of 12.8 ns, resulting in a PCR of 106.

In the context of radar applications, these results verify that our photonic approach is able to generate binary-phase-coded RF signals, and the resulting waveforms have the capability to increase the range resolution compared with the non-coded RF signals that have a constant PCR of 1, as shown in Figs. 6(a) and 6(b). In practice, the optimal length of a radar pulse and phase-coding scheme are determined by the required range resolution and receiver sensitivity of a particular application. However, to optimize the performance of PCR, e.g., to approximate the theoretical value of about 135 for the demonstrated bit length of this work, as shown in Figs. 6(c) and 6(d), the generated RF waveform should have a constant amplitude and a binary phase difference of 180°. For our approach, this means that further improvement of the RF signal performance requires reducing the waveguide loss of the MRM and providing an optimal value of MRM's power coupling coefficient κ that results in the relation of $\Delta\varphi_2 - \Delta\varphi_1 = 180°$.

We have experimentally demonstrated a photonic approach for the generation of binary-phase-coded RF signals at 35 GHz and 40 GHz, using a silicon microring modulator. The generated RF waveforms are proven to be applicable for pulse compression for radar applications. Recent PIC technologies offer a wide range of optoelectronic components, including lasers, modulators, amplifiers, and PDs [14]. The proposed photonic system has potential for being integrated on a single optical chip. This work points to the realization of a chip-scale flexible RF signal generator.

Funding. Australian Research Council (ARC) Laureate Fellowship scheme (FL 130100041).

REFERENCES

1. M. I. Skolnim, *Introduction to Radar* (McGraw-Hill, 1962), p. 101.
2. B. Razavi and R. Behzad, *RF Microelectronics* (Prentice Hall, 1998), p. 337.
3. E. I. Ackerman and A. S. Daryoush, IEEE Trans. Microwave Theory Tech. **45**, 1436 (1997).
4. Z. Li, W. Li, H. Chi, X. Zhang, and J. Yao, IEEE Photon. Technol. Lett. **23**, 712 (2011).
5. H. Chi and J. Yao, IEEE Photon. Technol. Lett. **19**, 768 (2007).
6. Y. Chen, A. Wen, Y. Chen, and X. Wu, Opt. Express **22**, 15618 (2014).
7. W. Li, L. X. Wang, M. Li, H. Wang, and N. H. Zhu, IEEE Photon. J. **5**, 5501507 (2013).
8. H. Chi and J. Yao, IEEE Microw. Wireless. Compon. Lett. **18**, 371 (2008).
9. C. Wang and J. Yao, IEEE Photon. Technol. Lett. **24**, 1493 (2012).
10. Z. Li, M. Li, H. Chi, X. Zhang, and J. Yao, IEEE Microw. Wireless. Compon. Lett. **21**, 694 (2011).
11. R. Wu, C. H. Chen, M. A. Seyedi, T. C. Huang, M. Fiorentino, R. Beausoleil, and K. T. Cheng, in *Integrated Photonics Research, Silicon and Nanophotonics* (2016), paper IW1B-4.
12. L. Zhuang, W. Beeker, A. Leinse, R. Heideman, P. van Dijk, and C. Roeloffzen, Opt. Express **21**, 3114 (2013).
13. X. Wu, C. Huang, K. Xu, C. Shu, and H. K. Tsang, IEEE Photon. Technol. Lett. **28**, 2058 (2016).
14. J. S. Fandiño, P. Muñoz, D. Doménech, and J. Capmany, Nat. Photonics **11**, 124 (2017).